AIAA AVIATION Forum
12-16 June 2023, San Diego, CA and Online
AIAA AVIATION 2023 Forum

10.2514/6.2023-3606

Enhancing Supersonic Rudder Control Surface Using Co-flow Jet Active Flow Control

Zhijin Lei * Gecheng Zha †
Dept. of Mechanical and Aerospace Engineering
University of Miami, Coral Gables, Florida 33124
E-mail: gzha@miami.edu

Abstract

This paper investigates the effects using high lift zero-net mass-flux Co-Flow Jet (CFJ) active flow control on aircraft control surfaces with rudders. The goal is to increase the control ability of rudder control surface of supersonic civil transport (SST) and save energy expenditure. A simplified Concorde vertical tail model is constructed and used as a baseline control surface for parametric trade study using a Reynolds-averaged Navier-Stokes (RANS) solver with Spalart-Allmaras (SA) model. A 3rd order WENO scheme for the inviscid flux is used to resolve the Navier-Stokes equations.

The 3D numerical studies indicate that, the Rudder-Stabilizer-CFJ, which was optimal CFJ configuration in two-dimensional simulation, generates jet flows that interfere with each other and thus no longer performs well in three-dimensional situation. The Rudder-CFJ is the optimal location, under which the optimal rudder deflection angle is 45°, and the optimal jet momentum coefficient is 0.08, which is the largest possible value. Under this condition, the maximum lift enhancement of 63.1% and the maximum $C_L/C_{D,c}$ increment of 18.1% is achieved. When the rudder deflection angle is 45°, lower C_μ will always generate positive lift enhancement and improves both C_L/C_D and $C_L/C_{D,c}$; at the lowest simulated C_μ=0.02, the improvements are 32.8% and 11.62% respectively. When the rudder deflection angle is larger than 45°, both lift coefficient and its increment drops. For this specific control surface geometry, CFJ does not reduce drag coefficient at all C_μs and all rudder deflection angles, but when the udder deflection angle is larger than 30° it still can improve both lift-drag ratio and corrected aerodynamic efficiency. CFJ supersonic aircraft rudder shows great potential to substantially reduce the size and weight of control surfaces with high control authority.

Nomenclature

AoA	Angle of Attack
AFC	Active Flow Control
C	Chord length
CFJ	Co-Flow Jet
VT	Vertical Tail
C_D	Drag coefficient
C_L	Lift coefficient
$C_{L,max}$	Maximum lift coefficient
C_M	Moment coefficient
C_p	Constant pressure specific heat

* Graduate Student
† Professor, ASME Fellow, AIAA associate Fellow

C_μ	Jet momentum coefficient, $\dot{m}_j\, U_j/(q_\infty\, S)$
D	Total drag on the rudder
$FASIP$	Flow-Acoustics-Structure Interaction Package
H_t	Total enthalpy
H	Height of the vertical tail (halfspan)
L	Total lift on the rudder
LE	Leading Edge
$\dot{m}$	Mass flow
M	Mach number
P	CFJ pumping power, $\dot{m}C_pT_{t,2}\ (\Gamma^{(\gamma-1/\gamma)}-1)/\eta$
P_c	Power coefficient, $P/0.5\rho_\infty {V_\infty}^3 S$
PR	Total pressure ratio, Γ
P_t	Total pressure
RANS	Reynolds-Averaged Navier-Stokes
Re	Reynolds number
S	Planform area of the vertical tail
TE	Trailing Edge
T_t	Total temperature
V_∞	Freestream velocity
ZNMF	Zero-Net Mass Flux
$(C_L/C_D)_c$	Aerodynamic efficiency corrected for CFJ, $C_L/(C_D+P_c)$
C_L^2/C_D	Productivity efficiency coefficient
$(C_L^2/C_D)c$	Productivity efficiency coefficient corrected for CFJ, $C_L^2/(C_D+P_c)$
c	Subscript, stands for corrected
j	Subscript, stands for jet
β	Sideslip angle
γ	Air specific heats ratio
η	CFJ pumping system efficiency, propeller efficiency
∞	Freestream density
δ	Deflection angle

1 Introduction

Supersonic Civil Transports (SST) remain a strong interest in the aviation research community and industry. Control surfaces like rudders, elevons and horizontal tails on such aircraft have their characteristics different from those on traditional commercial passenger jets.

"Conventional" SST designs, or those with a aerodynamic configuration similar to Concorde, use a large vertical tail to maintain their supersonic yaw stability, and a large rudder is introduced mainly to meet the requirement of control ability under cruise condition, where the drawback of low control force coefficients due to the low thickness and symmetric shape of the vertical tail profiles are cancelled out by the large absolute control force generated by high cruise speed of the aircraft. However, when it comes to takeoff and landing, the lower the flight speed is, the more difficult it usually will be to maintain the control ability on such rudders.

The nature of infrequent need of this application makes active flow control (ACT) preferable to passive control methods, which provides more than proportional control and frequently causes a drag penalty when the control is

not expected[1]. AFC methods has a long history of lift enhancing and drag reducing application[2, 3, 4, 5, 6, 7, 8], as well as enhancing the control performance of vertical tails. Sweeping jet is a unique method that has been widely used in vertical tail applications[9] and actual flight[10], and considered by NASA to be preferred than the method of synthetic jets[10, 11], which are made up of "ejection-suction" cycles of flow produced by orifices induced by moving diaphragms inside the control surface. Another notable AFC approach is the concept of Co-Flow Jet (CFJ) developed by Zha *et al*[12], which is a zero-net mass flux (ZNMF) flow control methodology that does not need to extract mass flow from inlet bleed of compressor secondary flow, and thus independent from the engine cycle. The theoretical and actual reliability of CFJ has been intensively validated both numerically and experimentally [12, 13, 14, 15, 16, 17, 18, 7, 19, 20, 21, 22], and great ability and potential to achieve radical lift augmentation, stall margin increase and drag reduction have been observed. Zhang *et al* [23] conducted a 2-D numerical simulation to study a new aircraft control surfaces using CFJ airfoils. Xu *et al* studied the energy expenditure based on Zhang *et al*'s results[24], and used 3-D Improved Delayed Detached Eddy Simulation (IDDES) turbulence model to simulate a 3-D vertical tail of a commercial passenger jet with airfoil of NACA0012[25].

There are not many published researches on applying AFC to wings or tails with thin profile. Mavris *et al*[26] employed circulation control(CC) flow control to enhance HSCT low speed lift coefficient based on the work of Englar[27]; with certain configurations, the CC method can reduce the takeoff field length by 31%, the liftoff speed by 11%, and the obstacle height speed by 10%. However, the jet flow of CC comes from engine bleed, which happen to be difficult to obtain during takeoff, when the engines need maximum mass flow for maximum thrust, and as well landing, when all the engines are expected idle. Lei *et al*[28, 29] numerically simulated applying CFJ on 2-D and 3-D flapped delta wings, and receive 50% lift enhancement and maintained lift-drag ratio at low speed. This method has been numerically proved to have a wide effective range of airfoil shapes[30]. The purpose of this paper is to apply CFJ to the vertical tail of a Concorde-like supersonic civil transport aircraft and improve its low-speed control ability.

1.1 The Co-Flow Jet Airfoil for Control Surfaces

In a CFJ airfoil, an injection slot near the leading edge (LE) and a suction slot near the trailing edge (TE) on the airfoil suction surface are created. As shown in Fig. 1, a small amount of mass flow is drawn into the suction duct, pressurized and energized by the micro compressor, and then injected near the LE tangentially to the main flow via an injection duct. The whole process does not add any mass flow to the system and hence is a zero-net-mass-flux(ZNMF) flow control.

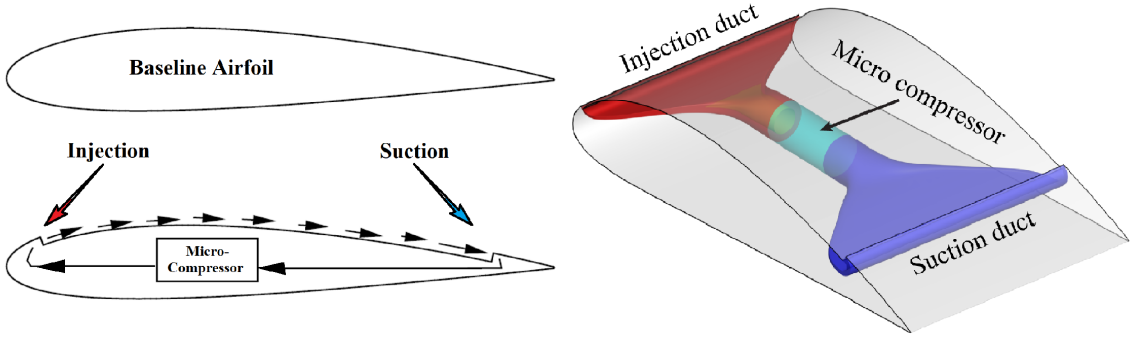

Figure 1: Schematic plot of a typical CFJ airfoil.

2 CFJ Parameters

This section lists important parameters to evaluate aerodynamic performance of a CFJ airfoil.

2.1 Jet Momentum Coefficient

The jet momentum coefficient C_μ is a parameter used to quantify the jet intensity. It is defined as:

$$C_\mu = \frac{\dot{m} U_j}{\frac{1}{2}\rho_\infty {U_\infty}^2 S} \tag{1}$$

where $\dot{m}$ is the injection mass flow, V_j is the mass-averaged injection velocity, ρ_∞ and V_∞ denote the free stream density and velocity, and S is the planform area.

2.2 Power Coefficient

CFJ is implemented by mounting a pumping system inside the wing that withdraws air from the suction slot and blows it into the injection slot. The power consumption is determined by the jet mass flow and total enthalpy change as the following:

$$P = \dot{m}(H_{t1} - H_{t2}) \tag{2}$$

where H_{t1} and H_{t2} are the mass-averaged total enthalpy in the injection cavity and suction cavity respectively, P is the Power required by the pump and $\dot{m}$ the jet mass flow rate. Introducing P_{t1} and P_{t2} the mass-averaged total pressure in the injection and suction cavity respectively, the pump efficiency η, and the total pressure ratio of the pump $\Gamma = \frac{P_{t1}}{P_{t2}}$, the power consumption is expressed as:

$$P = \frac{\dot{m} C_p T_{t2}}{\eta}(\Gamma^{\frac{\gamma-1}{\gamma}} - 1) \tag{3}$$

where γ is the specific heat ratio equal to 1.4 for air, the power coefficient is expressed as:

$$P_c = \frac{P}{\frac{1}{2}\rho_\infty V_\infty^3 S} \tag{4}$$

2.3 Corrected Aerodynamic Efficiency

The conventional wing aerodynamic efficiency is defined as $(\frac{C_L}{C_D})_c$. For the CFJ wing, the ratio above still represents the pure aerodynamic relationship between lift and drag. However, since CFJ active flow control consumes energy, the ratio above is modified to take into account the energy consumption of the pump. The formulation of the corrected aerodynamic efficiency for CFJ wings is:

$$(\frac{L}{D})_c = \frac{C_L}{C_D + P_c.} \tag{5}$$

where P_c is the power coefficient, L and D are the lift and drag generated by the CFJ wing. The formulation above converts the power consumed by the CFJ into a force $\frac{P}{V_\infty}$, which is added to the aerodynamic drag D. If the pumping power is set to 0, this formulation returns to the aerodynamic efficiency of a conventional wing.

3 Numerical Algorithm

The in-house high-accuracy CFD code Flow-Acoustics-Structure Interaction Package(FASIP), which has been intensively validated for CFJ simulations[4, 13, 14, 31, 16, 17, 18, 32, 7, 33, 34], is used in this simulation. The 3-D Reynolds averaged Navier-Stokes (RANS) equations with Spalart-Allmaras(SA) turbulence model is used. A 3rd order WENO scheme for the inviscid flux and a 2nd order central differencing for the viscous terms are employed to discretize the Navier-Stokes equations. The low diffusion E-CUSP scheme used as the approximate Riemann solver suggested by Zha *et al* [35] is utilized to evaluate the inviscid fluxes. Implicit time marching method using Gauss-Seidel line relaxation is used to achieve a fast convergence rate[36].

To achieve zero-net mass-flux with the CFJ flow control automatically in the solver, the injection mass flow is iterated to be made equal to the mass flow entering the suction slot. Additionally, the jet strength is controlled in order to reach the prescribed C_μ. This is achieved by iterating the jet total pressure until the C_μ value is within prescribed value tolerance. At the suction point, the suction mass flow is matched to the injection mass flow by iterating the static pressure at the suction cavity. The process is iterated throughout the simulation until the specified momentum coefficient is achieved and the injection and suction mass flow match.

4 Control Surface Definition

4.1 Baseline Model and Mesh Analysis

The baseline 3D vertical tail is built as a simplified vertical tail of Concorde. As a reasonable approximation, the baseline vertical tail uses a single symmetric airfoil of thickness 4.0%, the reference shape of which captured from the antenna blueprint of Technical Specification Manual of Concorde [37], as shown in Fig. 2:

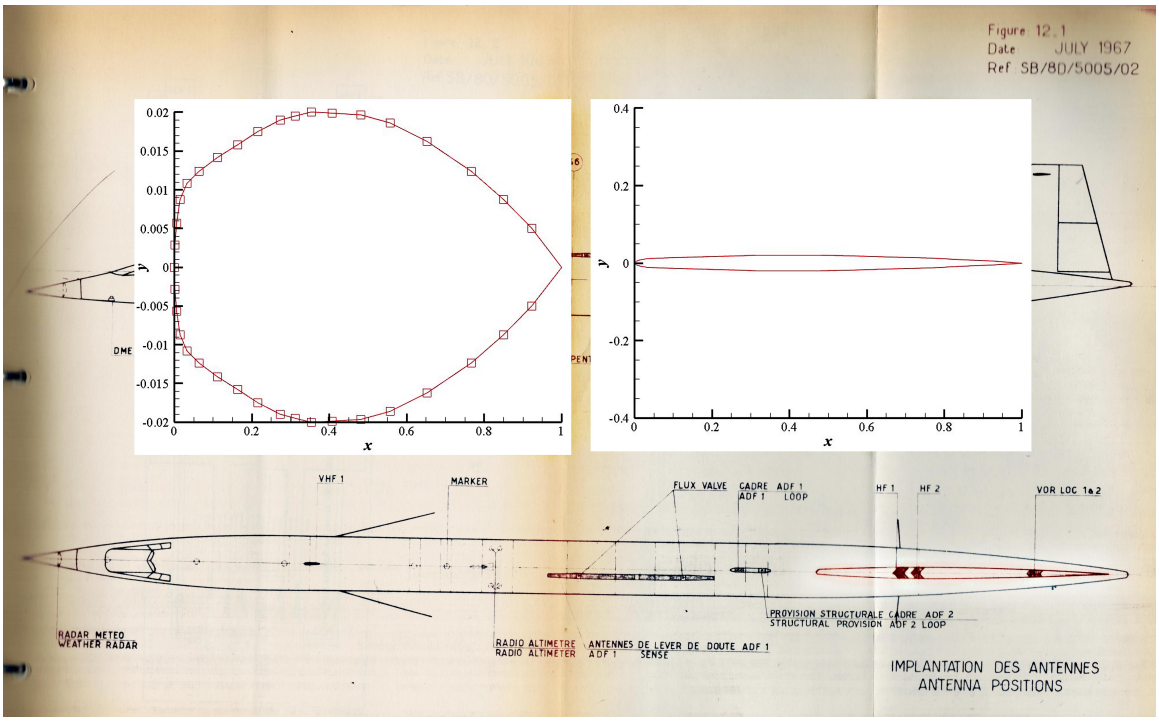

Figure 2: Baseline VT wing profile geometry, blueprint from [37].

According to the dimensions shown in Fig. 3(a) [37], a simplified baseline vertical tail planform is defined as the highlighted trapezoid shows, which has a LE swept angle of 42°, a height (span) of 5788.2 mm, a mean aerodynamic chord (MAC) of 7448.2 mm and a 20% chord of flap (rudder) length. Fig. 3(b) and (c) shows the planform shape differences between original (b) and simplified control surface(c). The baseline with a flap deflection angle of 30° is shown in Fig. 3(d), where the deflected mode of the control surface is geometrically simplified by deflecting the root and tip profile at 20% chord-length axis point separately and bridging the two profiles together.

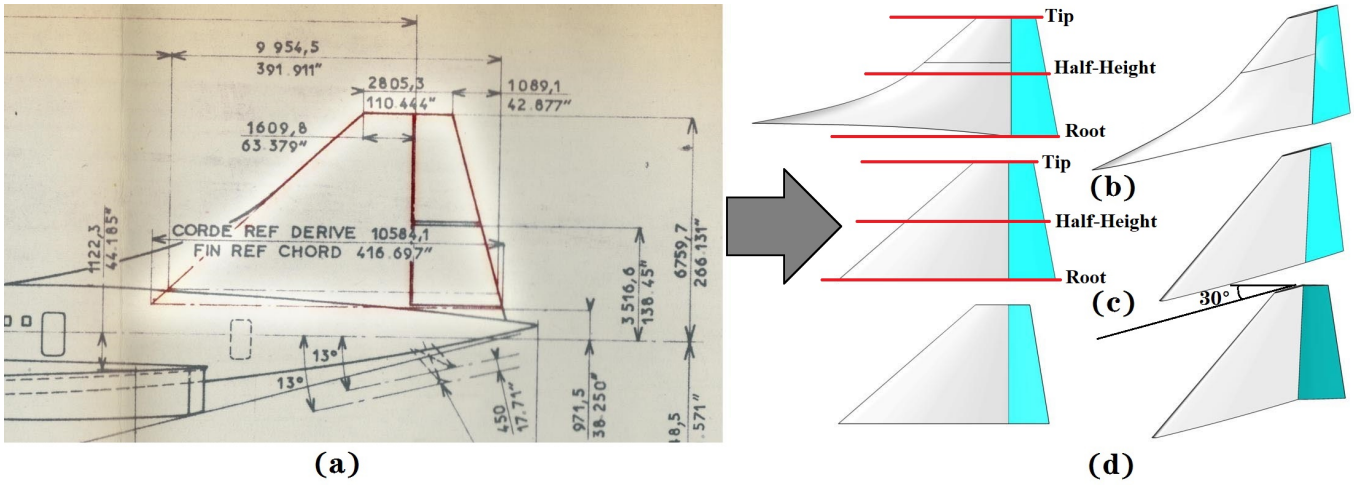

Figure 3: Dimension of a simplified Concorde vertical tail(a); a comparison between real Concorde VT(b), simplified model(c) and simplified model with rudder deflection angle of 30°(d).

The mesh topology is shown in Fig. 4. The computational domain is meshed using O-type grid with the mesh size of 6.80 million cells (1.03k $\times$ 60 $\times$ 100). Mesh in the streamwise direction is refined to precisely picture the shape of turning points and spaces for related CFJ-duct openings. The radial farfield has a distance of 21 times of the reference length (MAC) to the geometry, while the spanwise farfield has a distance of 10 times of the rudder height to the rudder tip.

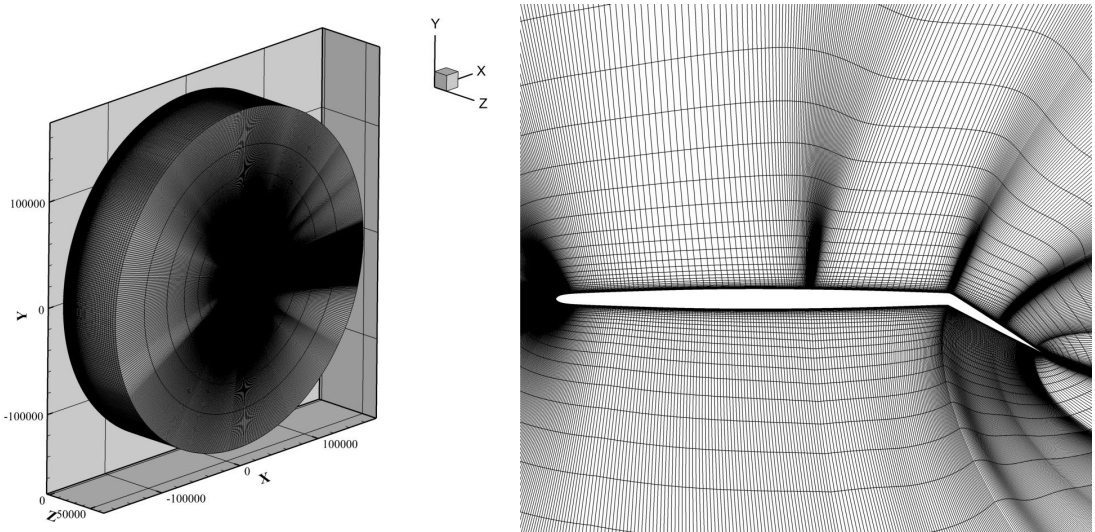

(a) Mesh in real dimension (mm)

(b) Mesh at root symmetric plane

Figure 4: 3-D Mesh calculation zone(a) and surface mesh of root symmetric plane(b).

The zero gradient condition is applied to farfield in the span direction away from the tip. The total pressure, total temperature and flow angle are specified at the farfield inlet and the static pressure is specified at the outlet to match the freestream Mach number. The symmetry boundary condition is applied to both the outer root domain and the farfield parallel to the tip surface. The no-slip wall boundary condition is applied to all solid wall surfaces, as shown in Fig. 5. The wall treatment suggested in [38] is employed to achieve the 3rd order accuracy.

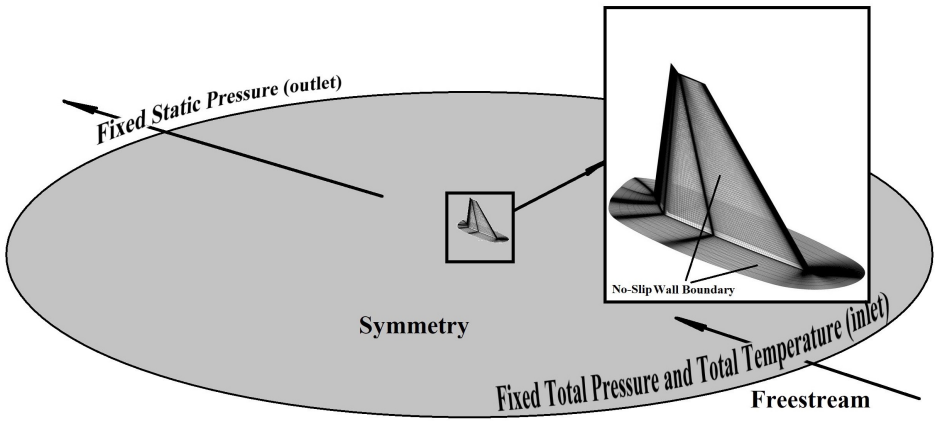

Figure 5: Definition of outer boundary conditions in the domains.

A mesh dependence analysis is conducted by doubling the number of grid points in $i-$, $j-$, and $k-$ direction respectively. Under the computational conditions of freestream $Re_\infty = 3.43 \times 10^7$ (based on MAC), $U_\infty = 68$m/s (Mach Number of 0.2), and sideslip angle β=0°, the mesh dependence results are shown in Table 1:

Table 1: Comparison of C_L, $C_L/C_{D,c}$ and other performances of baseline geometry, β=0°, δ=30°.

Case	Mesh size	C_L	C_D
Baseline	1.03k × 60 × 100	0.685	0.121
Doubled in i-direction	2.06k × 60 × 100	0.682	0.121
Doubled in j-direction	1.03k × 120 × 100	0.683	0.120
Doubled in k-direction	1.03k × 60 × 200	0.684	0.121

Results show that the maximum discrepancy for the lift coefficient is 0.43% and for the drag is 0.8%, which indicates that the baseline mesh is reasonably converged and is acceptable.

5 Study of Optimal CFJ Location

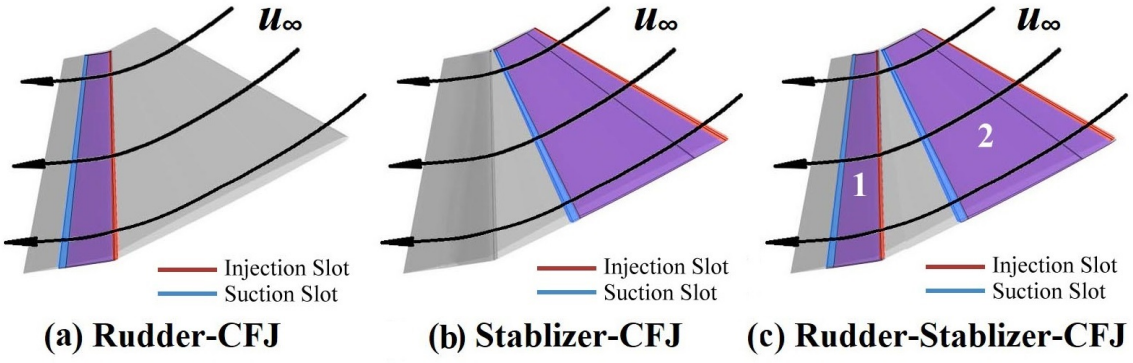

Figure 6: Three CFJ distribution locations with rudder deflection angle of 30°.

Three basic types of CFJ distribution locations are depicted as in Fig.6, namely Rudder-CFJ(Fig. 6(a)) "Stabilizer-CFJ"(Fig. 6(b)) and "Rudder-Stabilizer-CFJ"(Fig. 6(c)), where suction surfaces covered by CFJ jet flow are shown in purple. For stablizer-CFJ, the injection slot exit is located at 1%C from LE and the suction slot inlet is located at 51%C from LE. For rudder-CFJ, the injection slot starts from 80%C from LE(which is 2%C from rudder turning point) and the suction slot inlet is located at 90%C from LE(which is 12%C from rudder turning point). Two additional

For Stablizer-CFJ, the injection slot size is 12.0%C at all spanwise locations, and the suction slot size is 26.8%C at all spanwise locations, which is the maximum possible size allowed due to the geometrical limit. For Rudder-CFJ, the injection slot size is 6.0%C at all spanwise locations and the suction slot size is 10.0%C at all spanwise locations. In all CFJ geometries, the injection and suction slots in the opposite side will lead to a small gap, which is considered as insignificant to affect the aerodynamic performance and thus not simulated in this study. For boundary conditions inside the CFJ duct, constant static pressure is also used downstream inside the CFJ suction cavity, and the total pressure in the injection duct is iterated to meet the requirements of C_μ. The suction slot width and orientation are defined according to the best performing configuration of Liu *et al*[33].

The computational flow conditions of CFJ are identical to that of the baseline geometry, where the freestream Re_∞ equals to 3.43×10^7 (based on MAC), the freestream velocity $U_\infty = 68$m/s (Mach Number of 0.2), and the sideslip angle β=0°.

The performances of three configurations are listed in Table. 2. The result indicates that, when the rudder is deflected for 30°, at a C_μ of 0.08, Rudder-CFJ can increase C_L by 32.3% at around 7% cost of corrected L/D ratio, while the combined Rudder-Stabilizer-CFJ can increase C_L by 24.9% at around twice as that cost. Since it's not typical for rudder to deflect constantly with a sideslip angle β of 0° during cruise flight, $C_L/C_{D,c}$ decrease seems not as crucial as wing cases.

Table 2: Comparison of C_L, $C_L/C_{D,c}$ and other performances, β=0°, δ=30°, CFJ C_μ=0.08.

Type	C_L	ΔC_L	C_D	C_M	P_c	C_L/C_D	$C_L/C_{D,c}$	$\Delta C_L/C_{D,c}$
Baseline	0.685	-	0.121	0.131	0	5.661	5.661	-
Rudder-Stabilizer-CFJ	0.811	18.4%	0.127	-0.115	0.110	6.386	3.422	-39.6%
Rudder-CFJ	0.906	32.3%	0.146	0.192	0.026	6.206	5.267	-7.0%
Stabilizer-CFJ	0.939	37.1%	0.136	-0.113	0.121	6.904	3.654	-35.5%

6 Deflection Angle Study

The comparison of C_L, $C_L/C_{D,c}$ and other performances between baseline VT and Rudder-CFJ-VT with varied rudder deflection angle δs from 30° to 70° are shown as follows.

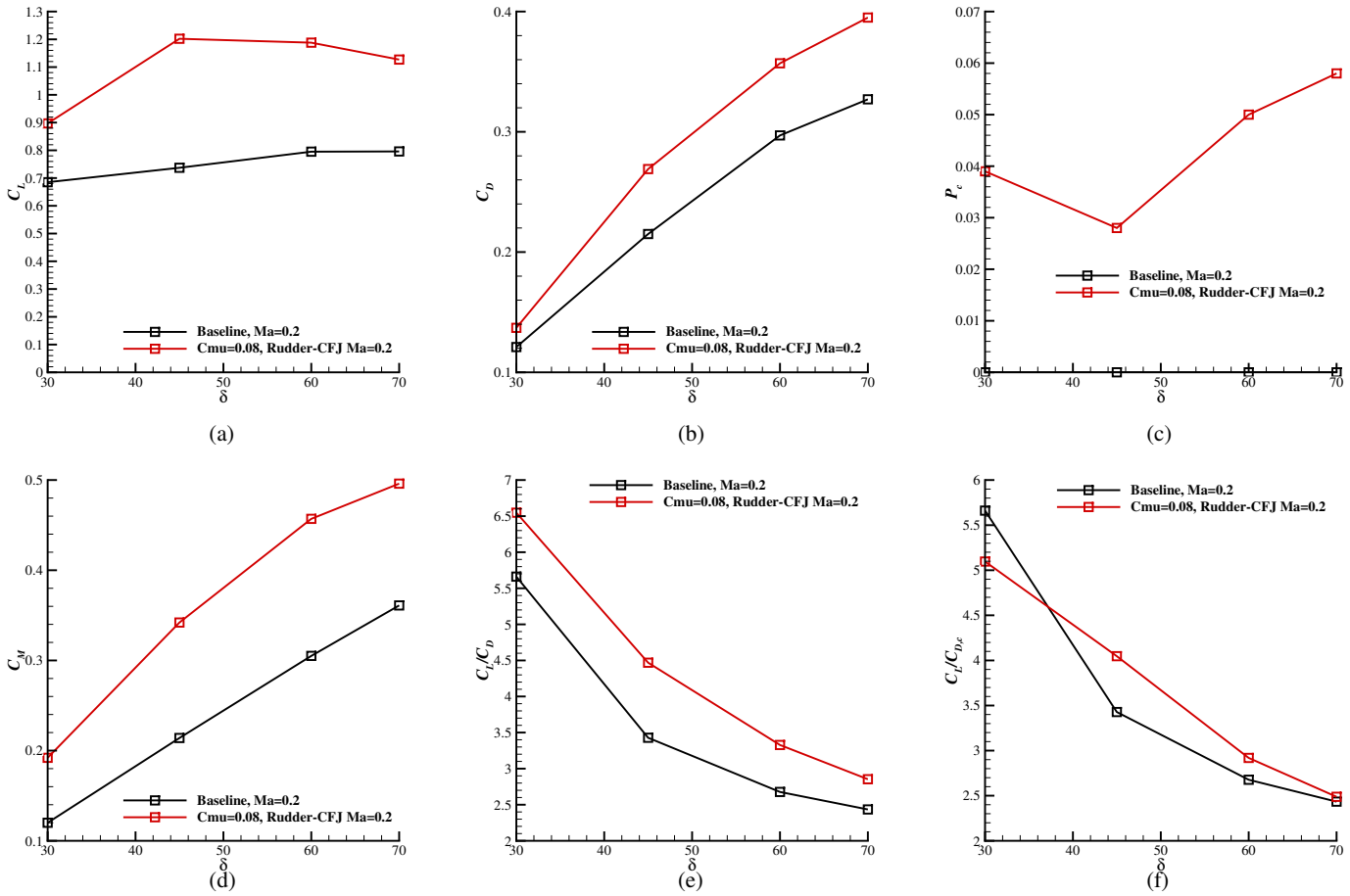

Figure 7: Comparison of C_L, $C_L/C_{D,c}$ and other performances between baseline VT and Rudder-CFJ-VT with varied δs, M=0.2, CFJ C_μ=0.08.

The result indicates that, when the rudder is deflected for 30°, at a C_μ of 0.08, Rudder-CFJ can increase C_L by 30.95% at around 10% cost of corrected L/D ratio, while the combined Rudder-Stabilizer-CFJ can increase C_L by 24.9% at around twice as that cost. Since it's not typical for rudder to deflect constantly with a sideslip angle β of 0° during cruise flight, $C_L/C_{D,c}$ decrease seems not as crucial as wing cases.

Table. 3 shows that, at rudder deflection angle δ=45°, C_L and $C_L/C_{D,c}$ reaches maximum simultaneously. At C_μ=0.08, the maximum C_L increase is 63.1%, while $C_L/C_{D,c}$ increase by 18.1% at the same time.

Table 3: Maximum increment of C_L and $C_L/C_{D,c}$, β=0°, CFJ C_μ=0.08.

Type	δ	C_L	C_L Improve	$C_L/C_{D,c}$	$\Delta C_L/C_{D,c}$
Max. C_L	45°	1.202	63.1%	4.047	18.1%
Max. $C_L/C_{D,c}$	30°	0.897	30.95%	5.068	-10.5%

Several 3-D and 2-D flowfields of Baseline-VT and Rudder-CFJ-VT with rudder deflection angle δ=45° are shown in Fig. 8 and Fig. 9 respectively. Similar flowfield situation as δ=30° is observed, but the separation is larger. In the baseline flowfield, separation can now be observed in tip region. When the rudder CFJ is applied,

small vortices still exist near the TE of rudder. When the rudder deflection angle δ is increased to 60°, CFJ can no longer control the separation near rudder, and the lift increase effect is weakened and mostly come from the energy-consuming jet effect.

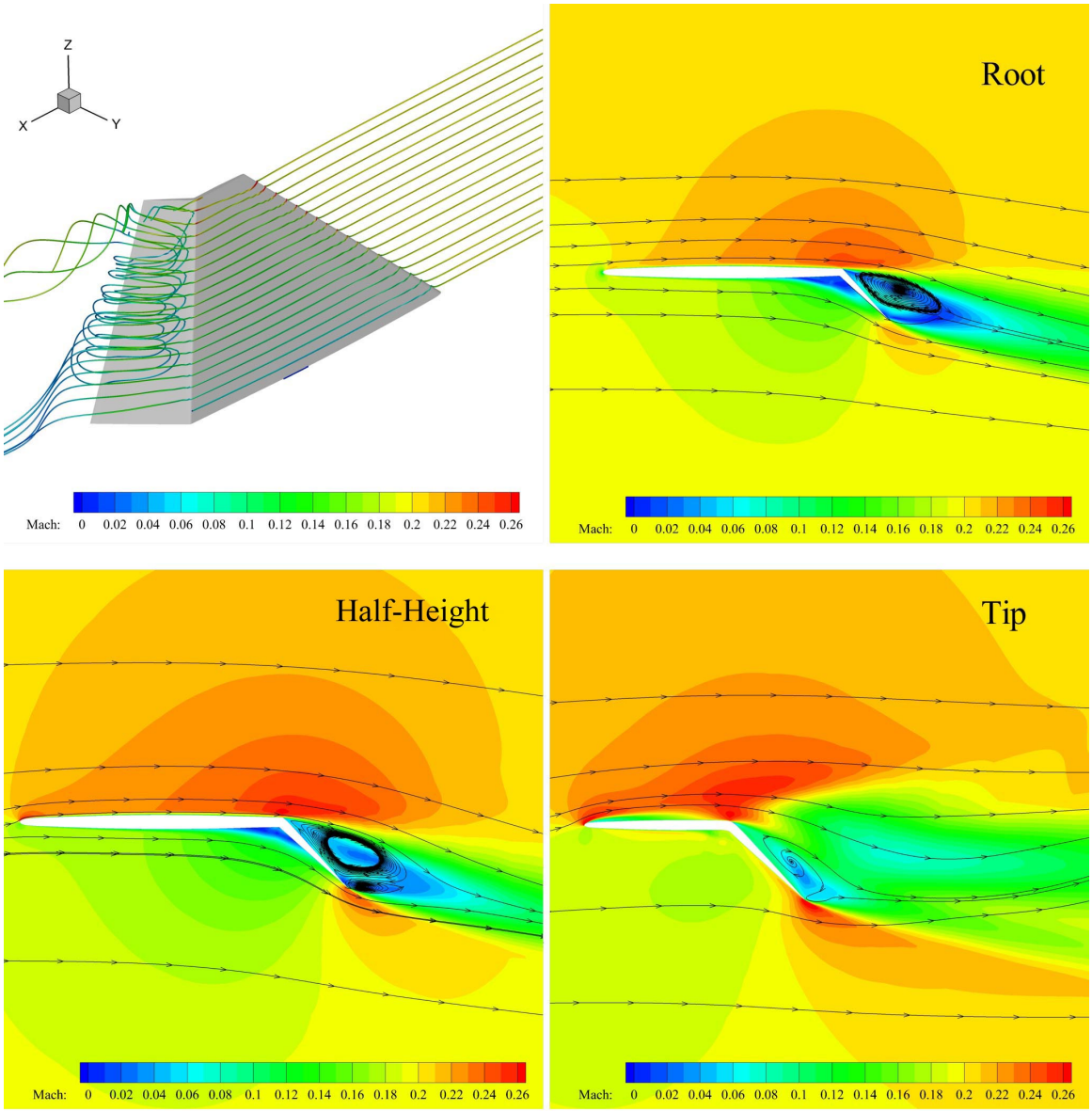

Figure 8: The streamline around baseline VT(a) and Mach number contours at root(b), half height(c) and tip(d) at δ=45°, Mach number of 0.2.

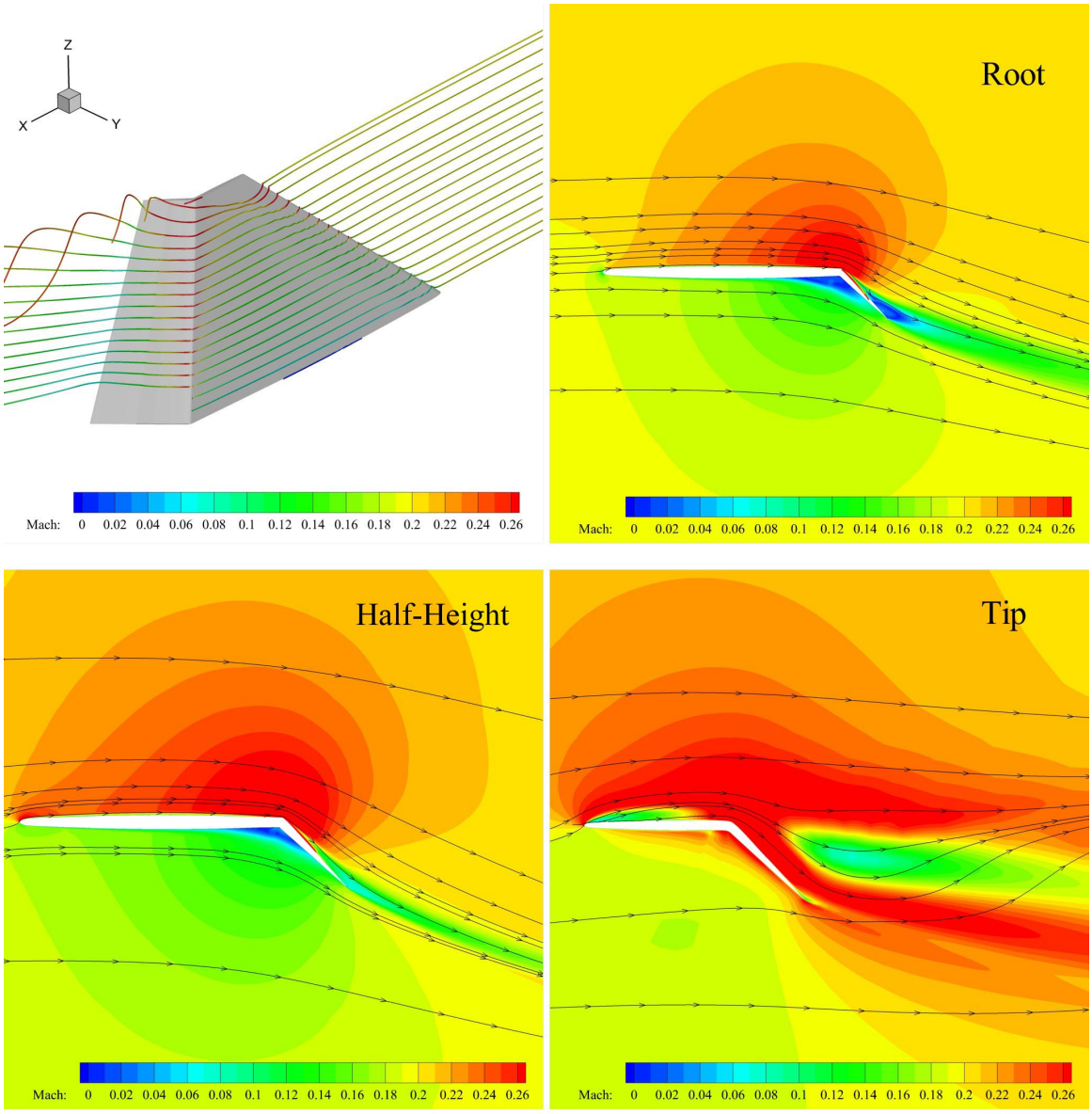

Figure 9: The streamline around Rudder-CFJ-VT(a) and Mach number contours at root(b), half height(c) and tip(d) at Mach number of 0.2, δ=45°, C_μ = 0.08.

7 Jet Momentum Coefficient Study

To study the effect of the jet intensity, four C_μs, namely 0.02, 0.04, 0.06 and 0.08 are simulated based on the configuration of Rudder-CFJ and constant δ=45°. All the flow conditions remain identical.

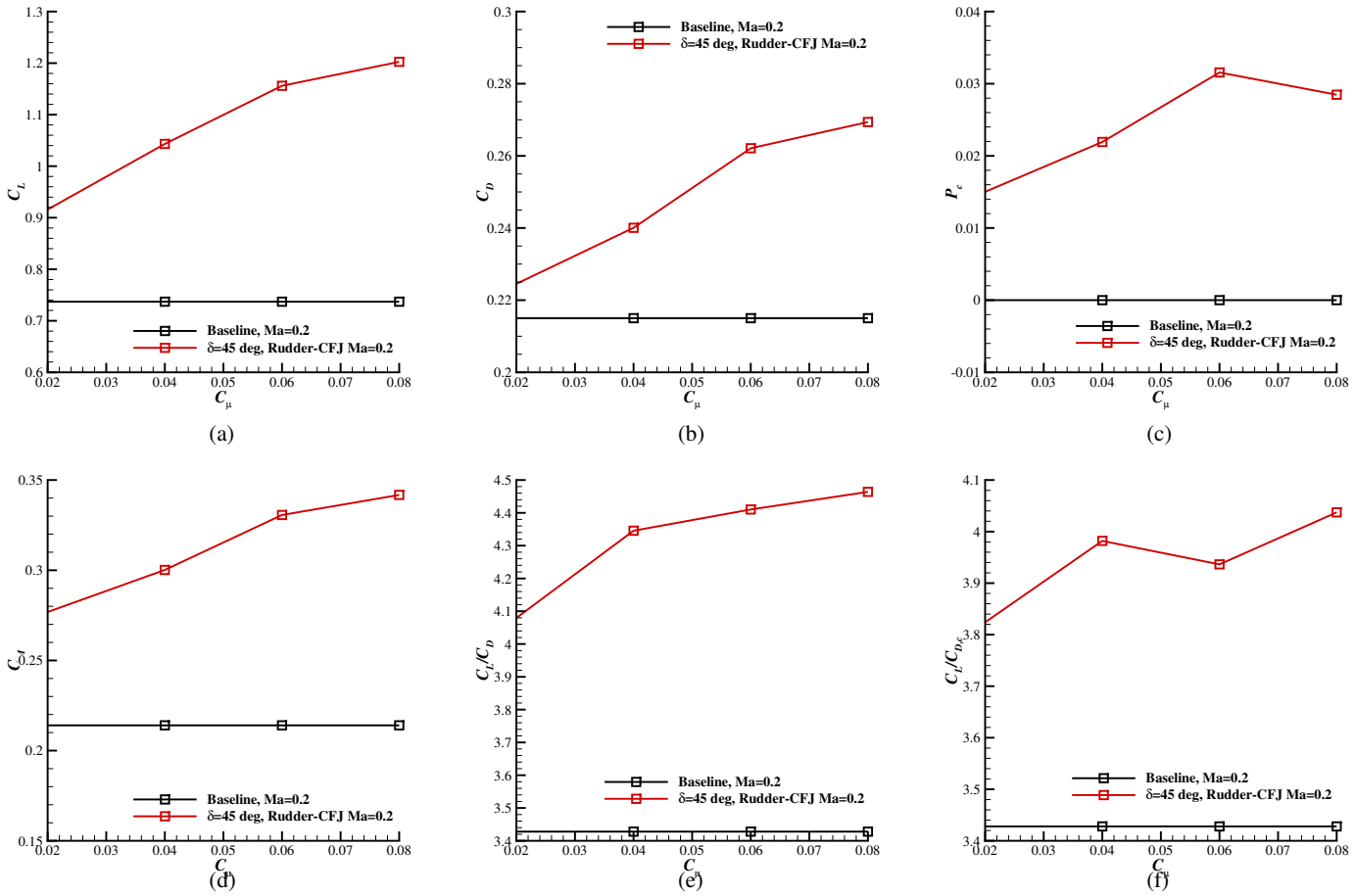

Figure 10: Comparison of C_L, $C_L/C_{D,c}$ and other performances between baseline VT and Rudder-CFJ-VT with varied C_μ, M=0.2, Flap deflection angle δ=45°.

As shown in Fig. 10, the results indicate that, at the flap deflection angle δ=45°, even at a minor C_μ of 0.02, there is still a 32.8% C_L increase, and $C_L/C_{D,c}$ is also increased by 11.62%. As C_μ goes larger, lift increases approximately linear, but the maximum power coefficient reaches peak at C_μ=0.06. Due to the nature of thin airfoil thickness, the suction slot cannot sustain a C_μ larger than 0.08 with mass flow convergence error less than 5%, so the optimal C_μ is considered as the largest possible C_μ=0.08, where both the maximum lift enhancement of 63.1% and the maximum $C_L/C_{D,c}$ increment of 18.1% is achieved. Streamlines around the control surface and flowfields' comparison at different cutaway planes are depicted from Fig. 11 to Fig. 14.

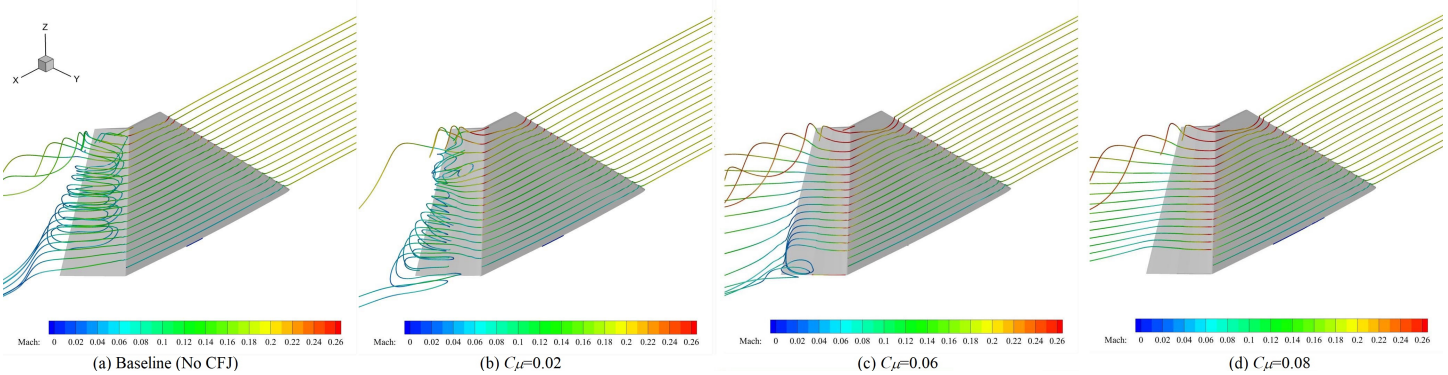

(a) Baseline (No CFJ) (b) C_μ=0.02 (c) C_μ=0.06 (d) C_μ=0.08

Figure 11: The streamline around vertical tails with different CFJ C_μs, namely: C_μ=0(baseline)(a);C_μ=0.02(b); C_μ=0.06(c) and C_μ=0.08(d). M=0.2, δ=45°.

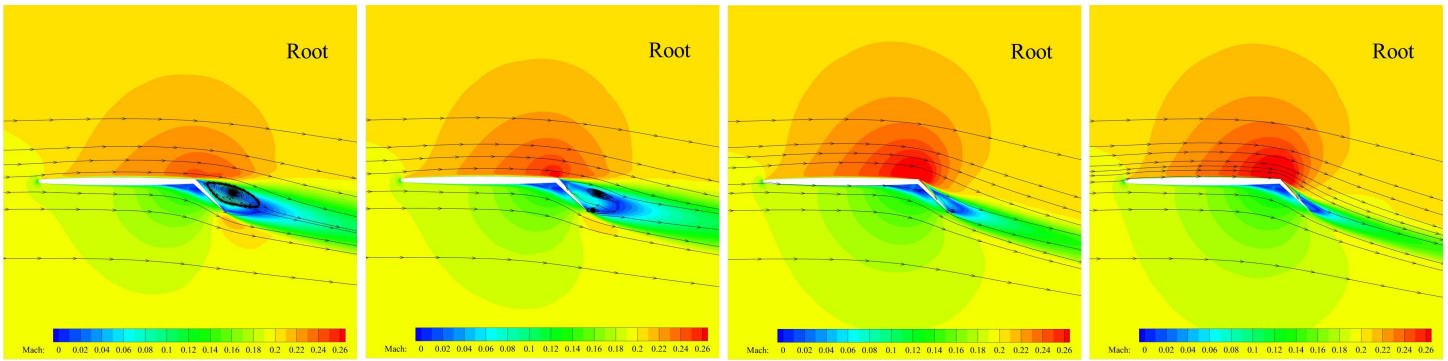

(a) Baseline (No CFJ) (b) C_μ=0.02 (c) C_μ=0.06 (d) C_μ=0.08

Figure 12: Mach number contours at root of vertical tails with different CFJ C_μs, namely: C_μ=0(baseline)(a);C_μ=0.02(b); C_μ=0.06(c) and C_μ=0.08(d). M=0.2, δ=45°.

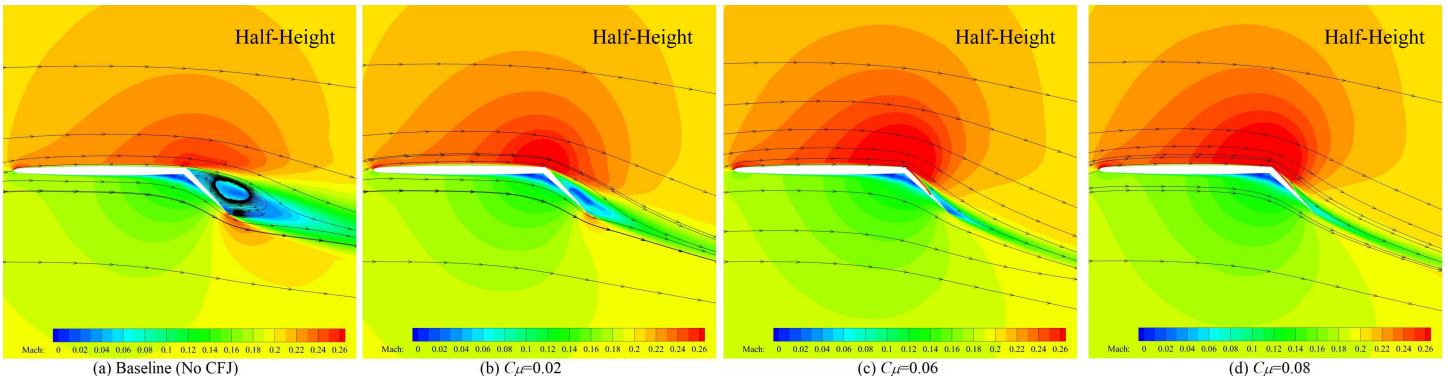

(a) Baseline (No CFJ) (b) C_μ=0.02 (c) C_μ=0.06 (d) C_μ=0.08

Figure 13: Mach number contours at half height of vertical tails with different CFJ C_μs, namely: C_μ=0(baseline)(a);C_μ=0.02(b); C_μ=0.06(c) and C_μ=0.08(d). M=0.2, δ=45°.

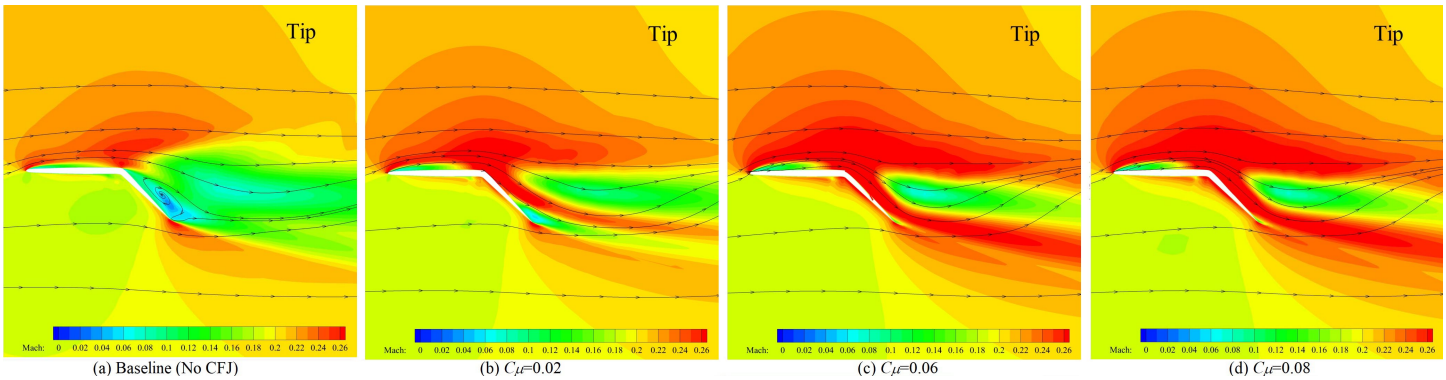

(a) Baseline (No CFJ) (b) C_μ=0.02 (c) C_μ=0.06 (d) C_μ=0.08

Figure 14: Mach number contours at tip of vertical tails with different CFJ C_μs, namely: C_μ=0(baseline)(a);C_μ=0.02(b); C_μ=0.06(c) and C_μ=0.08(d). M=0.2, δ=45°.

8 Conclusions

This paper investigates the effects using high lift zero-net mass-flux Co-Flow Jet (CFJ) active flow control on aircraft control surfaces with rudders. The goal is to increase the control ability of rudder control surface of supersonic civil transport (SST) and save energy expenditure. A simplified Concorde vertical tail model is constructed and used as a baseline control surface for parametric trade study using a Reynolds-averaged Navier-Stokes (RANS) solver with Spalart-Allmaras (SA) model. A 3rd order WENO scheme for the inviscid flux is used to resolve the Navier-Stokes equations.

The 3D numerical studies indicate that, the Rudder-Stabilizer-CFJ, which was optimal CFJ configuration in two-dimensional simulation, generates jet flows that interfere with each other and thus no longer performs well in three-dimensional situation. The Rudder-CFJ is the optimal location, under which the optimal rudder deflection angle is 45°, and the optimal jet momentum coefficient is 0.08, which is the largest possible value. Under this condition, the maximum lift enhancement of 63.1% and the maximum $C_L/C_{D,c}$ increment of 18.1% is achieved. When the rudder deflection angle is 45°, lower C_μ will always generate positive lift enhancement and improves both C_L/C_D and $C_L/C_{D,c}$; at the lowest simulated C_μ=0.02, the improvements are 32.8% and 11.62% respectively. When the rudder deflection angle is larger than 45°, both lift coefficient and its increment drops. For this specific control surface geometry, CFJ does not reduce drag coefficient at all C_μs and all rudder deflection angles, but when the udder deflection angle is larger than 30° it still can improve both lift-drag ratio and corrected aerodynamic efficiency. CFJ supersonic aircraft rudder shows great potential to substantially reduce the size and weight of control surfaces with high control authority.

9 Acknowledgment

The simulations are conducted on Pegasus super-computing system at the Center for Computational Sciences (CCS) at the University of Miami.

References

[1] B. L. Storms and C. S. Jang, "Lift enhancement of an airfoil using a gurney flap and vortex generators," *Journal of Aircraft*, vol. 31, no. 3, pp. 542–547, 1994.

[2] L. Pack, N. Schaeffler, C. Yao, and A. Seifert, "Active control of flow separation from the slat shoulder of a supercritical airfoil," in *1st Flow Control Conference*, p. 3156, 2002.

[3] S. Anders, W. Sellers III, and A. Washburn, "Active flow control activities at nasa langley," in *2nd AIAA Flow Control Conference*, p. 2623, 2004.

[4] G.-C. Zha, B. F. Carroll, C. D. Paxton, C. A. Conley, and A. Wells, "High-performance airfoil using coflow jet flow control," *AIAA journal*, vol. 45, no. 8, pp. 2087–2090, 2007.

[5] V. Kibens and W. W. Bower, "An Overview of Active Flow Control Applications at The Boeing Company." AIAA 2004-2624, June 2004.

[6] O. Kandil, E. Gercek, X. Zheng, and X. Luo, "Development of computational sensing and active flow control of airfoils during dynamic stall," in *42nd AIAA Aerospace Sciences Meeting and Exhibit*, p. 43, 2004.

[7] A. Lefebvre, B. Dano, W. Bartow, M. Difronzo, and G. Zha, "Performance and energy expenditure of coflow jet airfoil with variation of mach number," *Journal of Aircraft*, vol. 53, no. 6, pp. 1757–1767, 2016.

[8] T. Van Buren and M. Amitay, "Comparison between finite-span steady and synthetic jets issued into a quiescent fluid," *Experimental Thermal and Fluid Science*, vol. 75, pp. 16–24, 2016.

[9] N. W. Rathay, M. J. Boucher, M. Amitay, and E. Whalen, "Performance enhancement of a vertical tail using synthetic jet actuators," *AIAA journal*, vol. 52, no. 4, pp. 810–820, 2014.

[10] J. C. Lin, M. Y. Andino, M. G. Alexander, E. A. Whalen, M. A. Spoor, J. T. Tran, and I. J. Wygnanski, "An overview of active flow control enhanced vertical tail technology development," in *54th AIAA aerospace sciences meeting*, p. 0056, 2016.

[11] M. Y. Andino, J. C. Lin, A. E. Washburn, E. A. Whalen, E. C. Graff, and I. J. Wygnanski, "Flow separation control on a full-scale vertical tail model using sweeping jet actuators," in *53rd AIAA aerospace sciences meeting*, p. 0785, 2015.

[12] G.-C. Zha and D. C. Paxton, "A Novel Flow Control Method for Airfoil Performance Enhancement Using Co-Flow Jet." *Applications of Circulation Control Technologies*, Chapter 10, p. 293-314, Vol. 214, Progress in Astronautics and Aeronautics, AIAA Book Series, Editors: Joslin, R. D. and Jones, G.S., 2006.

[13] G.-C. Zha, W. Gao, and C. Paxton, "Jet Effects on Co-Flow Jet Airfoil Performance," *AIAA Journal, No. 6,*, vol. 45, pp. 1222–1231, 2007.

[14] G.-C. Zha, C. Paxton, A. Conley, A. Wells, and B. Carroll, "Effect of Injection Slot Size on High Performance Co-Flow Jet Airfoil," *AIAA Journal of Aircraft*, vol. 43, 2006.

[15] G.-C. Zha, B. Carroll, C. Paxton, A. Conley, and A. Wells, "High Performance Airfoil with Co-Flow Jet Flow Control," *AIAA Journal*, vol. 45, 2007.

[16] Wang, B.-Y. and Haddoukessouni, B. and Levy, J. and Zha, G.-C., "Numerical Investigations of Injection Slot Size Effect on the Performance of Co-Flow Jet Airfoil," *Journal of Aircraft*, vol. Vol. 45, No. 6,, pp. pp.2084–2091, 2008.

[17] B. P. E. Dano, D. Kirk, and G.-C. Zha, "Experimental Investigation of Jet Mixing Mechanism of Co- Flow Jet Airfoil." AIAA-2010-4421, 5th AIAA Flow Control Conference, Chicago, IL, 28 Jun - 1 Jul 2010.

[18] B. P. E. Dano, G.-C. Zha, and M. Castillo, "Experimental Study of Co-Flow Jet Airfoil Performance Enhancement Using Micro Discreet Jets." AIAA Paper 2011-0941, 49th AIAA Aerospace Sciences Meeting, Orlando, FL, 4-7 January 2011.

[19] A. Lefebvre, G-C. Zha, "Numerical Simulation of Pitching Airfoil Performance Enhancement Using Co-Flow Jet Flow Control," *AIAA paper 2013-2517*, June 2013.

[20] A. Lefebvre, G-C. Zha, "Cow-Flow Jet Airfoil Trade Study Part I : Energy Consumption and Aerodynamic Performance," *32nd AIAA Applied Aerodynamics Conference, AIAA AVIATION Forum, AIAA 2014-2682*, June 2014.

[21] A. Lefebvre, G-C. Zha, "Cow-Flow Jet Airfoil Trade Study Part II : Moment and Drag," *32nd AIAA Applied Aerodynamics Conference, AIAA AVIATION Forum, AIAA 2014-2683*, June 2014.

[22] Lefebvre, A. and Zha, G.-C., "Trade Study of 3D Co-Flow Jet Wing for Cruise Performance." AIAA Paper 2016-0570, AIAA SCITECH2016, AIAA Aerospace Science Meeting, San Diego, CA, 4-8 January 2016.

[23] J. Zhang, K. Xu, Y. Yang, Y. Ren, P. Patel, and G. Zha, "Aircraft control surfaces using co-flow jet active flow control airfoil," in *2018 applied aerodynamics conference*, p. 3067, 2018.

[24] K. Xu, J. Zhang, and G. Zha, "Drag minimization of co-flow jet control surfaces at cruise conditions," in *AIAA Scitech 2019 Forum*, p. 1848, 2019.

[25] K. Xu and G. Zha, "3d aircraft control surface enabled by co-flow jet flap," in *AIAA AVIATION 2022 Forum*, p. 3889, 2022.

[26] D. Mavris and M. Kirby, "Takeoff / landing assessment of an hsct with pneumatic lift augmentation," in *37th Aerospace Sciences Meeting and Exhibit*, p. 534, 1998.

[27] R. L. L. Englar, "Circulation control for high lift and drag generation on stol aircraft," *Journal of Aircraft*, vol. 12, no. 5, pp. 457–463, 1975.

[28] Z. Lei and G. Zha, "Lift enhancement for highly swept 3d delta wing at low speed using coflow jet flow control," in *AIAA AVIATION 2021 FORUM*, p. 2559, 2021.

[29] Z. Lei and G. Zha, "Lift enhancement of supersonic thin airfoil at low speed by co-flow jet active flow control," in *AIAA AVIATION 2021 FORUM*, p. 2591, 2021.

[30] Z. Lei and G. Zha, "Numerical investigation of low speed performance of a curved co-flow jet supersonic airfoil," in *AIAA SCITECH 2023 Forum*, p. 0243, 2023.

[31] Yang, Yunchao and Zha, Gecheng, "Super-Lift Coefficient of Active Flow Control Airfoil: What is the Limit?," *AIAA Paper 2017-1693, AIAA SCITECH2017, 55th AIAA Aerospace Science Meeting, Grapevine, Texas*, p. 1693, 9-13 January 2017.

[32] A. Lefebvre and G-C. Zha, "Conceptual Design of an Electric Airplane Utilizing Co-Flow Jet Flow Control," *AIAA Paper 2015-0772, 53rd AIAA Aerospace Sciences Meeting*, Jan 2015.

[33] Z. Liu and G. Zha, "Transonic airfoil performance enhancement using co-flow jet active flow control," in *8th AIAA Flow Control Conference*, p. 3472, 2016.

[34] Z. Lei and G. Zha, "Axis-symmetric mixed-compression supersonic inlet bleed via a zero-net-mass-flux co-flow jet flow control," in *AIAA SCITECH 2022 Forum*, p. 2234, 2022.

[35] Zha, G.C., Shen, Y.Q. and Wang, B.Y., "An improved low diffusion E-CUSP upwind scheme ," *Journal of Computer and Fluids*, vol. 48, pp. 214–220, Sep. 2011.

[36] G.-C. Zha and E. Bilgen, "Numerical Study of Three-Dimensional Transonic Flows Using Unfactored Upwind-Relaxation Sweeping Algorithm," *Journal of Computational Physics*, vol. 125, pp. 425–433, 1996.

[37] B. Corp., "Technical specs manual of concorde," 1968.

[38] Y.-Q. Shen, G.-C. Zha, and B.-Y. Wang, "Improvement of Stability and Accuracy of Implicit WENO Scheme ," *AIAA Journal*, vol. 47, pp. 331–344, 2009.